Biophys J BioFAST, published on January 16, 2008 as doi:10.1529/biophysj.107.122796

This unedited manuscript has been accepted for publication in Biophysical Journal and is freely available on BioFast at http://www.biophysj.org. The final copyedited version of the paper may be found at http://www.biophysj.org.

# Volume exclusion in calcium selective channels

**Dezső Boda[*,†,1], Wolfgang Nonner[‡], Douglas Henderson[§], Bob Eisenberg[*], and Dirk Gillespie[*]**

[*]Department of Molecular Biophysics and Physiology, Rush University Medical Center, Chicago IL 60612
[†]Department of Physical Chemistry, University of Pannonia, H-8201 Veszprém, P. O. Box 158, Hungary
[‡]Department of Physiology and Biophysics, Miller School of Medicine, University of Miami, Miami FL 33101
[§]Department of Chemistry and Biochemistry, Brigham Young University, Provo UT 84602

[1]Author to whom correspondence should be addressed. E-mail address: dezso_boda@rush.edu



Copyright 2008 by The Biophysical Society.

**Abstract**

Corry, Chung and their associates have proposed an interesting model for calcium channel selectivity. However, on the basis of their reported results we find it impossible to assess the merits of their model because their results and claims concerning selectivity are based on an extrapolation over four orders of magnitude to low $Ca^{2+}$ concentration. Their results and claims have been presented in several articles and reviews in several journals and, thus, need attention. In this paper, we first establish that we obtain results on electrostatics and channel occupancies similar to the high-concentration simulations they present. We then perform grand canonical ensemble simulations that enable us to study micromolar $Ca^{2+}$ concentrations. We find that their model channel is only weakly $Ca^{2+}$ selective. A crucial problem with their model appears to be the placement of the negatively charged glutamate structural elements in fixed positions inside the protein rather than as flexible units inside the filter.

*Key words:* Ca channel, Ionic selectivity, Volume exclusion, $Ca^{2+}$ binding, Monte-Carlo simulation, Modeling

# Introduction

Ion channels are essential for the proper function of cells and organisms (1). The task of ion channels is to pass ions through their pore selectively. In particular, calcium (Ca) channels play an important role in vital physiological functions such as neurotransmitter release, muscle contraction, cell signaling, and many others. Ca channels selectively conduct $Ca^{2+}$ ions when these are present in millimolar or larger concentration even if other ions ($Na^+$ or $K^+$) are present in a much larger quantity. On the other hand, $Ca^{2+}$ ions block the current of monovalent ions when $Ca^{2+}$ is present at a lower concentration. This $Ca^{2+}$-block occurs in the L-type Ca channel at micromolar $Ca^{2+}$ concentrations (2–6). Several attempts to explain the mechanisms of these important selectivity phenomena have been made in the literature. A study of one model is given in this paper with the goal of obtaining a better understanding of the behavior of $Ca^{2+}$-selective channels.

In the past few years, our understanding of Ca channels has dramatically improved. Nonner et al. (7, 8) (NCE) have proposed a simple intuitive model, based on a theory of homogeneous fluids, in which the selectivity of a particular cation selective channel (the Ca channel in this study) produced by the competition between the attractive Coulombic interactions of the cations with the net negatively charged structural elements of the channel filter and the repulsive excluded volume of the ions and structural elements in a small volume. In this competition cations are attracted into the filter but, because of the restricted geometry of the channel and the excluded volume of the ions and channel structural elements, divalent ($Ca^{2+}$) ions are more effective at balancing the -4$e$ negative charge of the selectivity filter of the Ca channel than are monovalent ($Na^+$) ions since they deliver twice the charge while occupying almost the same volume. Thus, the $Ca^{2+}$ ions preferentially occupy the filter even when the concentration of the $Ca^{2+}$ ions in the surrounding reservoir is several orders of magnitude smaller than the concentration of $Na^+$ ions in this reservoir. This model can be extended to sodium (Na) channels (9, 10).

This appealing mechanism for selectivity can be called *charge/space competition* (CSC) and is not only intuitively attractive but is in accord with thermodynamics. In contrast to a mechanical system, where the stable state is the state with the lowest *energy*, a stable thermodynamic system is the state with the lowest *free energy*, $A = U - TS$, where $U$ is the thermodynamic energy, $T$ is the temperature, and $S$ is the entropy. The minimum in $A$ is the result of the competition between $U$ and $S$. In general, attractive forces contribute to $U$ and volume exclusion forces, due to particle size, contribute to $S$. This division is absolute in the well-known van der Waals theory that is a useful starting point for a theory of a liquid and is quite accurate in more

refined theories of liquids (11). In the context of a channel, Coulombic forces contribute primarily to $U$ while the volume exclusion forces due to the size of the particles contribute primarily to $S$.

The CSC mechanism accounts not only for the selectivity of $Ca^{2+}$ versus $Na^{+}$ ions in Ca and Na channels but accounts for the selectivity of cations on the basis of ion diameter. The CSC mechanism has been applied to the ryanodine receptor Ca channel, where it reproduces or predicts more than 50 data curves (12, 13). The intuitive ideas of NCE have been made rigorous by means of the continuously refined studies of Boda *et al.* (14–16) (Bea). In these studies, we have made Monte Carlo (MC) simulations that most recently have included the effects of charge polarization due to dielectric boundaries (17, 18) and, by means of grand canonical (GC) ensemble MC simulations, have been able to obtain results for exceedingly low concentrations ($10^{-6}$ M) of $Ca^{2+}$ ions. The statistical sampling in the filter is enhanced by means of preferential sampling (14).

A second approach, due to Corry *et al.* (Cea) (19–22), also describes the channel using an idealized geometry (the structure of the Ca channel is not known). The ions move in a dielectric continuum solvent and the wall of the channel protein forms a dielectric boundary. Cea used Brownian dynamics (BD) simulations at high (typically $\pm$200 mV) applied voltages to calculate the current flowing through the channel and extrapolate their results to the low Ca concentrations that are of physiological interest. Cea state that their model reproduces the micromolar $Ca^{2+}$ vs. $Na^{+}$ selectivity of the L-type Ca channel. These claims have been stated several times in different places and deserve examination. Their bold extrapolation needs particular attention.

This paper analyzes consequences of two crucial differences between the Cea and Bea approaches.

1. Cea performed BD simulations at rather high $Ca^{2+}$ ion concentrations (greater than 18 mM). Their claim that their model reproduces micromolar $Ca^{2+}$-selectivity is based on a large extrapolation (four orders of magnitude) to the low $Ca^{2+}$ concentrations of interest. In contrast, we simulate micromolar concentrations directly using the GC ensemble. In this work, simulating the micromolar regime directly, we show that the model of Cea does not have the strong $Ca^{2+}$-selectivity properties that Cea have extrapolated.

2. Another significant difference between the Bea and Cea approaches is that Cea place the negative structural charges of the selectivity filter behind the wall in fixed positions. This rigid model is in sharp contrast with the flexible environment in the selectivity filter of our model. In the studies using the CSC mechanism (7–10, 12–18) the oxygens of the glutamate side chains are treated

as mobile structural ions that are restricted to the selectivity filter but otherwise free to move inside the filter. Thus, these ions form a liquid-like self-adjusting environment for the passing $Na^+$ and $Ca^{2+}$ ions. Cea claim that in their model selectivity is due *only* to Coulomb forces. Quoting from page 308 of their review (21), "Indeed, the electrostatic attraction of the protein is all that is required to account for ion permeation and selectivity in this model". We argue that electrostatics alone is not sufficient to produce micromolar selectivity in the Cea model and that excluded volume effects cannot be ignored. By placing the structural ions inside the selectivity filter, the $Ca^{2+}$-selectivity of the model can be improved.

The simulation results of Cea have been presented without critique in many reviews (6, 20–22). The objective of this paper is to report direct simulation results in the $Ca^{2+}$ concentration range where Cea have extrapolated and where in experiments $Ca^{2+}$ block is observed. Presenting simulation results with a CSC model of the filter embedded in the Cea channel geometry permits us to draw conclusions for the possible mechanism of selectivity as viewed by the Cea group and us.

# The models

We adopt the standard usage in statistical mechanics and distinguish between a *model*, which is defined by a Hamiltonian that gives the energy of the system in terms of the particle positions and momenta and their interaction with any fixed boundaries in the system and a *method*, a theory or in our case a simulation, that permits the study of the consequences of a model.

## The model of Cea

**Geometry.** The Cea model is shown in Fig. 1A and consists of a rotationally symmetric channel that is a cylinder of length 50 Å with a variable radius that defines the boundary of the channel (see Fig. 1 of Ref. (19)). The $z$ axis of the coordinate system is along the central axis of the channel cylinder. The cylinder is centered about $z = 0$ and extends from -25 Å to 25 Å. The region in the interval -25 Å $< z <$25 Å that is beyond the channel wall is the channel protein. At its most narrow part (10 Å $< z <$15 Å), the radius of the channel is 2.8 Å. This region represents the selectivity filter. The region $|z| >$25 Å are the two reservoirs of the system. Each reservoir is a cylinder of radius 30 Å with a height of about 33 Å. The walls of the confining simulation cell are hard.

Cea use what they call a *stochastic* boundary at the far ends of the reservoirs, whose purpose is to maintain the two reservoirs at constant concentration. It means that once an ion crosses the channel, say, from right to left, another ion is transplanted from the left hand side of the simulation cell to right hand side in a position where it does not overlap with other ions. The applicability of this step without a grand-canonical acceptance test of the new position of the ion, which ensures that the chemical potential of the system has not been changed, is questionable. Cea performed a check (23) following Im et al. (24) and demonstrated that they obtain the same results with the two methods. Nevertheless, they used a simpler channel and high concentrations in their test.

The structural elements of the channel (glutamates in the case of a calcium channel) are modeled as *fixed* point (fractional) charges of magnitude -0.811$e$ that are 1 Å *inside* the protein arranged in a spiral at the channel filter (the red spheres in Fig. 1A). Additional positive and negative fractional charges ($\pm 0.374e$) form dipoles (yellow and blue spheres in Fig. 1A) at the intracellular entrance of the channel to decrease the large dielectric barrier for the passing ions.

The region outside the protein and within the channel contains the electrolyte. Only the ions in the electrolyte are modeled explicitly. Water is represented by a dielectric continuum. The dielectric coefficients of the electrolyte and protein are taken to be 60 and 2, respectively.

In our implementation of the Cea model we have a different cell and procedure; we use a much larger cell (a radius of 64 Å and length of 300 Å). Our simulations are performed by MC using the GC ensemble rather than BD. Thus, we do not need the questionable stochastic boundary to maintain the reservoir concentrations. Instead, the GC ensemble allows us to simulate micromolar bath concentrations without introducing statistical bias. These points are discussed in more detail below. For the sake of comparison with Cea, in implementing their model, we used the values of Cea for the energetic parameters (the values for the parameters in Eqs. 1-4) and did not concern ourselves with the question of whether these are the optimal values.

**Ion-wall potential.** We describe the short-range interaction of an ion and the channel wall by

$$u_i^{\mathrm{IW}}(r) = \frac{F_0}{9} \frac{(R_i + R_{\mathrm{W}})^{10}}{(R_{\mathrm{W}} + r)^9}, \tag{1}$$

where $F_0 = 2 \times 10^{-10}$ Newtons, $R_i$ is the radius of the ion (the value of $R_i$ for $Ca^{2+}$, $Na^+$, and $Cl^-$ are 0.99 Å, 0.9 Å, and 1.81 Å, respectively), $R_{\mathrm{W}} = 1.4$ Å is the radius of the atoms making up the wall, and $r$ is the perpendicular distance of an ion from the nearest portion of the

protein wall.[2]

Our Eq. 1 differs from Eq. 4 of Cea (19), where $(R_c(z) + R_W - a)^9$ appears in the denominator ($R_c(z)$ is the channel's radius as a function of $z$ and $a$ is the ion's distance from the $z$-axis). Eq. 4 of Cea does not give an inverse 9 relation to normal distance between ion and wall when the angle of the tangent of the surface and the $z$-axis is larger than zero. Furthermore, using this radial distance, the ion-wall potential is not defined for the region where the surface is perpendicular to the $z$-axis. This is the region near the protein wall in the reservoir ($|z| > 25$ Å), where Cea applied a hard wall to prevent the ions from crossing the surface of the protein. We used Eq. 1 because it gives the same potential everwhere near the protein surface; therefore, it is more consistent than the one used by Cea. In the selectivity filter (our main region of interest) the two equations are equivalent.

**Ion-ion potential.** The Cea ion-ion interaction is taken to be the pairwise sum of Coulomb interactions plus a short range interaction,

$$u_{ij}^{\mathrm{SR}}(r_{ij}) = U_{ij}^0 \left\{ \left( \frac{R_{ij}^{\mathrm{c}}}{r_{ij}} \right)^9 - \exp\left( \frac{R_{ij}^{\mathrm{h}} - r_{ij}}{c_{\mathrm{e}}} \right) \cos\left( 2\pi \frac{R_{ij}^{\mathrm{h}} - r_{ij}}{c_{\mathrm{W}}} \right) \right\}, \tag{2}$$

where the contact distance is $R_{ij}^{\mathrm{c}}$=$R_i + R_j$ for cation-anion pairs, while it is $R_{ij}^{c}$=$R_i + R_j + 1.6$ Å for like ions, the origin of the hydration force is $R_{ij}^{\mathrm{h}} = R_{ij}^{\mathrm{c}} \pm 0.2$ Å (positive for like ions and negative otherwise), $c_{\mathrm{W}} = 2.76$ Å, and $c_{\mathrm{e}} = 1$ Å. The values of $U_{ij}^0$ are 16.8, 8.5, 1.7, 2.5, 0.8, and 1.4 $kT$ for $Ca^{2+}$-$Cl^-$, $Na^+$-$Cl^-$, $Ca^{2+}$-$Na^+$, $Na^+$-$Na^+$, $Ca^{2+}$-$Ca^{2+}$, and $Cl^-$-$Cl^-$ pairs, respectively. The potential parameters were fitted to the potentials of mean force given by Guàrdia et al. (25–27)

The presence of the repulsive inverse 9 term in Eq. 2 seems to disagree with the assertion of Cea that volume exclusion forces do not play a role in their model. If this assertion were valid, the first term would be unnecessary.

The purpose of the sum of the repulsive $1/r^9$ potential and the exponentially decaying oscillating hydration force is to mimic the results of molecular dynamics (MD) simulations. Cea assert that the radial distribution functions (RDFs) for NaCl that result from the use of Eq. 2 are similar to those obtained by Lyubartsev and Laaksonen (28) by

[2]Eq. 1 is referred to as the 'usual' inverse 9 repulsive potential. Some comment is required. The 'usual' inverse 9 potential is applicable to a flat surface of infinite extent. It is obtained by integration over half space of a repulsive inverse 12 potential between the volume elements of the flat surface and a given particle located a perpendicular distance outside this surface. Its application to a cylinder with a small radius and a finite length is questionable.

a self-consistent iteration involving a molecular dynamics (MD) simulation.

Cea find that the locations of the maxima in their RDFs roughly match those of the MD RDFs. Matching the location of the maxima only requires that the effective ion diameters be reasonable. The height of the maximum is a much more important issue that is not mentioned in the paper of Cea. The maximum of the $Na^+$-$Cl^-$ RDF obtained from the Cea model significantly underestimates the maximum obtained from the MD simulation. As a matter of fact, it can be seen in Fig. 2 of Ref. (19) by Cea that this maximum is lower than the first maximum of the $Na^+$-$Na^+$ pair. It is a strange electrolyte, indeed, where like ions attract each other more strongly than cation-anion pairs. Figure 3 of Ref. (28) by Lyubartsev and Laaksonen shows the opposite behavior.

Cea claim that "simpler ion-ion interactions ... are not suitable for use in calcium channels" because "they allow cations to pass each other in the selectivity filter, thus making it impossible to explain the observed blocking of sodium ions by calcium, and vice versa". It is our belief that explanation of $Ca^{2+}$-block of $Na^+$-current in Ca channels does not require single filing (more about this later) (7, 12). Thus, the above reasoning for using Eq. 2 cannot be accepted. Ions do not enter the narrow channel with their whole hydration shell, therefore the potential fitted to bulk simulation results cannot be applied.

**Born energy.** The ions in the Cea model experience a change in Born energy at the axial locations where the pore joins the baths ($z_c = -22.5$ Å and $z_c = 22.5$ Å). The Born energy change upon entering the pore is

$$E_i^B = \frac{q_i^2}{8\pi\epsilon_0 R_i^B}\left(\frac{1}{\epsilon} - \frac{1}{80}\right) \tag{3}$$

where $\epsilon = 60$ is the dielectric constant in the channel and $R_i^B$ is the Born radius of the ion species $i$ of charge $q_i$. In the Cea model, the transition of Born energy is smoothed over a 3 Å interval centered on $z_c$ using the interpolation

$$u_i^B(s) = \frac{E_i^B}{16}(3s^5 - 10s^3 + 15s + 8), \tag{4}$$

where $s = (z - z_c)/(1.5\text{Å})$ for the left boundary, and $s = -(z - z_c)/(1.5\text{Å})$ for the right boundary.

Cea refer to their earlier paper (29) for further description on this method, but we found the value of $E_i^B$ only for $K^+$ ion. Therefore, we used Born radii fitted to experimental hydration energies reported in the literature (30) (-1608.3, -423.7, and -304.0 kJ/mol for $Ca^{2+}$, $Na^+$,

and $Cl^-$, respectively). The corresponding $E_i^B$ values in $kT$ (at 298 K) are 2.737, 0.721, and 0.517 for $Ca^{2+}$, $Na^+$, and $Cl^-$, respectively.

Cea qualify this procedure of accounting for the difference in the polarization properties of pore and bath as a "compromise". In reality, the ions induce charge on the dielectric boundary between pore and baths. The interaction of every ion with that charge should be calculated in a self-consistent treatment. Simulation of ions crossing dielectric boundaries is difficult, which is the reason of the "compromise" used by Cea. With the dielectric boundary effects described by the Born energy, Cea solve the electrostatics using a dielectric coefficient of 60 for the baths, which might produce unrealistically large ion-ion interactions in the bath solutions.

## The CSC model

We also study a realization of the CSC model. Here the structural charges of the EEEE locus are placed *inside the lumen of the channel* rather than into a rigid channel wall (Fig. 1B). The channel is otherwise kept identical to that of Cea in order to focus the comparison on the difference in the placement of charged groups. The terminal carboxylate groups of the glutamate residues are represented in the CSC model as 8 half-charged oxygen ions. Each oxygen ion is a hard sphere with radius 1.4 Å. The oxygen ions are allowed to overlap with the wall of the filter, but their center cannot approach the wall closer than 0.5 Å. These oxygen ions, that now are part of the electrolyte filling the filter, are confined by a cylinder with radius 3.7 Å and length 9.352 Å. They are confined to be within this volume but are otherwise free to move in this space. The oxygen ions interact with other charges in the simulation cell through the Coulomb potential. They interact with other ions (including other oxygen ions and counter-ions) through the hard sphere potential instead of the soft-core potential in Eq. 2. The hard-core radii used for $Na^+$, $Ca^{2+}$, and $Cl^-$ were 1, 0.99, and 1.81 Å (31). (The soft-core potential is still used for pairs of $Na^+$, $Ca^{2+}$, and $Cl^-$ ions because we wish to convert the Cea to the CSC type of model without making other changes.) The oxygen ions are not subject to the soft interaction potential with the channel wall in Eq. 1.

In the CSC model the glutamate groups occupy filter space and they accommodate to the movement of passing cations so the grand potential of the system is minimized. Note that these structural charges now are in the dielectric domain of the solution space, whereas in the Cea model they are in the dielectric of the pore wall. This has consequences for the polarization charge produced by these structural ions on the protein/pore interface.

## Simulation method

MC simulations were performed in the grand canonical ensemble (32, 33) using the Metropolis sampling. Details of our sampling are described in reference (18). In brief, our attempts for moving a particle included: (1) small changes in position (we use only this movement to displace oxygen ions in the CSC model), (2) large changes in position, (3) a preferential change between positions in the channel and bath subvolumes, (4) insertion/removal of a neutral group of ions ($Na^+$ and $Cl^-$, or $Ca^{2+}$ and $2Cl^-$) into/from the simulation cell (32), and (5) a GC attempt similar to (4) but involving preferred subvolumes of the simulation cell ($Na^+$ and $Ca^{2+}$: the pore region; $Cl^-$: the whole simulation cell). The acceptance criterion for preferential MC step (3) considered the volume ratio of the respective regions. It was shown that this MC step accelerates sampling considerably (14).

The preferential GC step (5) is an additional variety of MC attempt not used in our previous works (9, 17, 18). It was included to accelerate convergence toward equilibrium in these simulations. Without this step, we equilibrated the bulk region of the simulation cell with an external bath of fixed chemical potentials (and thus with fixed salt concentrations) and then we equilibrated the channel region with this bulk region using the preference sampling of step (3). The basic idea of the new method is that we can equilibrate the channel region with the external bath directly without applying the intermediate step of equilibration with the bulk region of the cell. If a system is in equilibrium with an external bath, any subsystem of it is also in equilibrium with the external bath. Therefore, we can insert cations directly into the pore and thus increase the percentage of MC steps occuring between the pore and the external bath.

An example of convergence is shown in Fig. 2, where the number of $Ca^{2+}$ and $Na^+$ ions in the selectivity filter ($10 < z < 15$ Å) is plotted versus the index of the attempt. The bath concentration of $Ca^{2+}$ in this test was $10^{-5}$ M, a value important for the purpose of this paper. The convergence of the simulation is much faster when the preferential GC step (5) is used (note the logarithmic scale of the abscissa). A production run comprised $6 \times 10^8$ to $1.2 \times 10^9$ attempts.

In GC simulations, bath concentrations are a computed consequence of the chemical potentials assigned to the ions in the system. We determined chemical potentials needed to establish targeted bath concentrations using an iteration (34). The reported bath concentrations are the average ion concentrations in the bulk-like regions of our large baths.

In the BD simulations of Cea, the charges induced by ions on the dielectric boundaries were computed using a boundary element method (35). The contributions of these charges to the field were computed by

an iterative method and tabulated for a set of ion positions; during the BD simulation, the field contributions were estimated from the tabulated values using interpolation considering the actual ion positions. This method was chosen for computational efficiency.

In our MC simulation, we solve the electrostatics by a boundary element method (18, 36), which we called the Induced Charge Computation (ICC) method. Rather than using an iterative method we generate the LU-decomposition of the matrix that results from the boundary integral equations. Since boundaries are fixed in space during our simulation, this computation can be done as part of the overhead at the beginning of the simulation. Specific solutions are obtained for each particle distribution during the MC simulation using backsubstitution. Thus our computation of potential does not involve interpolations like those used by Cea. We divide the boundary surface into 1811 (generally curved) 'tiles' (outlined by the grid shown in Fig. 1) and use an accurate method to include surface curvature into the computation of the electrostatics (18). Our simulation cell is considerably larger (radius 64 Å, length 300 Å) than that used by Cea. This cell typically contains about 300 $Na^+$. Thus, the baths in our simulations approximate bulk conditions.

# Results and Discussion

## Profiles of potential energy and ion concentrations

Cea have computed potential energies in a test in which a single $Na^+$ or $Ca^{2+}$ was used to probe the pore along the $z$ axis; the ion was allowed to find lowest energy positions in the cross-section of the pore (Fig. 5 of Ref. (19)). These results allow us to compare our different methods used to compute the electrostatics. The lines of Fig. 3 represent the results of Cea; the symbols are computed with our method. The agreement is very good. We had expected to find differences because we estimated some details of the surface geometry that were not numerically specified in Ref. (19). The agreement confirms the validity of both numerical approaches for the Cea model.

It is unfortunate for a comparison with equilibrium simulations that Cea presented axial concentration profiles only for conditions that produced ion flow (an applied voltage of -200 or +200 mV; Figs. 9 and 10 of Ref. (19)). Figure 4 shows superpositions of the Cea non-equilibrium profiles and equilibrium profiles (corresponding to zero applied voltage) that we computed with the MC method. Cea find rather small differences between the $Na^+$ profiles for -200 and +200 mV, so that we might expect to find a profile that is well bracketed by those of Cea. This is the case (Fig. 4A).

The difference between the Cea profiles for $Ca^{2+}$ between the two voltages is much larger than for $Na^+$ (Fig. 4B). Our equilibrium profile differs from both profiles computed by Cea. The difference is smaller for the $Ca^{2+}$ distribution on the sink side than on the source side of the Cea non-equilibrium distributions. This is consistent with the conclusion of Cea that $Ca^{2+}$ conduction in their model is limited by a substantial dielectric barrier that arises in the cavity region of the model pore. When ions flow this barrier causes an accumulation of $Ca^{2+}$ on the source side of the barrier, above any accumulation that occurs in equilibrium. With these considerations, we feel that the ion distributions obtained by Cea under conditions of flow and our equilibrium results are mutually consistent.

## The anomalous mole fraction effect

A signature of Ca channel conduction is the anomalous mole fraction effect (AMFE) first observed in whole-cell currents (2, 37) and subsequently in currents recorded from individual Ca channels (38). When the extracellular $Ca^{2+}$ concentration is less than $10^{-7}$ M but the $Na^+$ concentration is 30-150 mM, the Ca channel conducts a $Na^+$ current. Increasing the $Ca^{2+}$ concentration into the micromolar range reduces the current carried by $Na^+$ by an order of magnitude. Only if the $Ca^{2+}$ concentration is raised to the millimolar level, does the channel preferentially conduct $Ca^{2+}$ (reviewed in Ref. (6)). The AMFE appears to be less strong (that is, the current is less reduced in the presence of micromolar $Ca^{2+}$) when the membrane voltage is $\leq -50$ mV (39).

Cea have used BD simulation results obtained with rather large concentrations of $Ca^{2+}$ ($\geq 18$ mM) at the applied voltage of -200 mV to extrapolate to the $Ca^{2+}$ concentration and voltage ranges where the AMFE has been experimentally observed. They find nearly perfect agreement with the experimental observation of Almers et al. (2), that 0.9 $\mu$M $Ca^{2+}$ reduces $Na^+$ current to half that observed when $Ca^{2+}$ concentration is $10^{-8}$ M or less. These experimental currents were measured between -20 and +7 mV applied voltage; in experiments at low $Ca^{2+}$ concentrations ($< 10^{-4}$M) symmetrical $Na^+$ concentrations of 32 mM were present. The extrapolation to low $Ca^{2+}$ concentrations used by Cea was described as based on entry and exit rates of $Ca^{2+}$ simulated at high [$Ca^{2+}$] but no mathematical description of the procedure was provided in their paper. The extrapolation to experimental voltages is questionable because it is unknown whether the physical conditions underlying the AMFE arise in a biological channel tested at -200 mV. Experiments are done at voltages much smaller in magnitude than -200 mV. Indeed, Fukushima and Hagiwara (39) found that the AMFE is substantially weakened when the test voltage is $\leq -50$ mV.

Fig. 5A shows the computed AMFE curves of Cea (lines) super-

imposed on the published experimental points of (3) (*circles* — please note that Fig. 16B of (19) shows 'a representation' of these data in which the reduction of the $Na^+$ current by $Ca^{2+}$ is complete, whereas the data of (3) show incomplete reduction). The reduction of $Na^+$ current found by Cea in the extrapolated AMFE is complete. These extrapolated simulation results of Cea have been presented in several reviews (6, 20–22) but have not been corroborated by a direct calculation. Our MC method using the grand canonical ensemble permits us to directly simulate $Ca^{2+}$ concentrations in the range where the experimental AMFE is observed. We have re-examined $Ca^{2+}$ binding as the basis for an AMFE in the Cea model using this independent and direct simulation method.

Our results obtained for a range of $Ca^{2+}$ concentration added to a 0.15 M NaCl bath are summarized in Fig. 5B. These results, obtained for the GC ensemble, indicate that the model accumulates $Ca^{2+}$ far less avidly than the extrapolated computations of Cea suggested. About 0.2 mM $Ca^{2+}$ are required in the bath in order to displace one half of the $Na^+$ ions from the pore (see the arrow in Fig. 5B). Cea extrapolated a half-point near $10^{-6}$ M $Ca^{2+}$. At $10^{-6}$ M $Ca^{2+}$, we detect a very small concentration of $Ca^{2+}$ in the selectivity filter of the Cea model; the total occupancy by $Ca^{2+}$ in the filter region is about 0.007. The blockade that Cea have predicted by extrapolation would require that one $Ca^{2+}$ would be have to be present in the filter region at least one half of the time.

Figure 6 shows axial concentration profiles for several of the $Ca^{2+}$ concentrations that were included in the summary presented in Fig. 5B. We detect no significant accumulation anywhere in the model pore when bath $Ca^{2+}$ concentration is 1 $\mu$M. On the other hand, $Na^+$ profiles are hardly influenced by the presence of 1 $\mu$M $Ca^{2+}$ in the bath. Thus the results of our MC simulations do *not* support the conclusion of Cea, that their model accounts for the experimental AMFE.

Our MC simulations are restricted to equilibrium (zero applied voltage). This condition is included in the range of experimental voltages where the AMFE is observed, whereas the voltage simulated by Cea is far outside the experimental range. (Neither simulation includes the $Ca^{2+}$ gradient present in the experiments.) It seems possible that the AMFE extrapolated by Cea does occur in their model, as a consequence of the strong applied voltage: $Ca^{2+}$ might be accumulated up to a large local concentration near the intracellular end of the filter (compare Fig. 4B) because inward flow of $Ca^{2+}$ is restricted by a high electrostatic barrier in the central cavity of the Cea model channel. To the extent that this voltage-driven accumulation of $Ca^{2+}$ is *required* for AMFE behavior, the Cea model is not adequate. The fact that the AMFE occurs at negative and positive voltages of small magnitude is experimentally established (2, 37, 38). (Note, however, that all

these experiments involve strong asymmetry in $Ca^{2+}$ concentrations and some involve asymmetries in monovalent cation concentrations and/or species.)

Cea state that the AMFE requires that the ions be described by hydrated-ion force fields, which increase ion diameters to the extent that a $Na^+$ ion is unlikely to pass a $Ca^{2+}$ ion in the filter. An alternate mechanism for the AMFE, not depending on the single-file restriction or excessive voltage but involving depletion of an ion species from a region of the channel, has been described generically (40) and in L-type and RyR Ca channels (7, 12). In three cases, a hitherto unknown AMFE has been predicted by theory as an effect of ion depletion and subsequently been found by experiment (12, 13).

The electrostatic barrier in the cavity region apparently limits $Ca^{2+}$ current to unrealistically small values. The simulated $Ca^{2+}$ currents (Fig. 5A, *open squares*) are much smaller than the experimental currents (*filled circles*). Moreover, the $Na^+$ and $Ca^{2+}$ branches of the simulation results in Fig. 16A of Ref. (19) (reproduced in our Fig. 5A) have been separately normalized and the authors state that 'the magnitude of the calcium current is significantly lower than that for sodium'. Thus, the Cea pore model also gives unrealistic results for the Ca branch of the AMFE curve.

The weak $Ca^{2+}$ affinity that we find for the Cea model under equilibrium conditions might underlie an excessive block of $Ca^{2+}$ inflow in the presence of extracellular $Na^+$ that Cea have observed in their BD simulations. Fig. 17 of Ref. (19) shows that extracellular $Na^+$ blocks simulated $Ca^{2+}$ currents supported by a bath concentration of 150 mM $Ca^{2+}$. In the experiments of Polo-Parada and Korn (41) (which are quoted by Cea), extracellular $Na^+$ partially blocks inward current when the extracellular $Ba^{2+}$ concentration is 1mM but $Na^+$ has little blocking effect when the extracellular $Ba^{2+}$ concentration is 10mM (Fig. 6 of Ref. (41)). $Ca^{2+}$ is thought to bind more strongly than $Ba^{2+}$ in Ca channels (38).

## The CSC model of the EEEE locus produces stronger $Ca^{2+}$ affinity than the Cea model

The Cea model involves a rigid structure for the functional groups that chelate $Ca^{2+}$: these groups are embedded in a hard pore wall. We have tested the possibility that this restriction is excessive and actually limits $Ca^{2+}$ affinity to the low level that our simulations have revealed. We test a CSC model in which the carboxylate groups of the EEEE side chains are modeled by tethered half-charged oxygen anions that are allowed to associate freely with counterions within the volume of the selectivity filter (Fig. 1B). The only restriction to their motion is that they cannot leave the pore section that we call 'filter'. Thus

the structural anions of the model channel behave like the particles of a confined fluid. This model of the selectivity filter has been proposed by some of us and has been studied using a variety of methods (7–10, 12–18). To make comparisons of the CSC and Cea models clearer, we change only the description of the charged groups but otherwise maintain the Cea description of the system (see Methods).

Simulation results concerning competitive $Ca^{2+}$ and $Na^{+}$ accumulation in the CSC selectivity filter are shown in Fig. 7 (*closed symbols*). The simulation results obtained with the Cea model are also shown for comparison (*open symbols*). Allowing the structural anions to interact with ions in a liquid-like setting greatly increases the $Ca^{2+}$ affinity of the model. Regarding the AMFE, we note that a $Ca^{2+}$ bath concentration of only 5 $\mu$M suffices to displace one half of the $Na^{+}$ that is accumulated in the absence of $Ca^{2+}$, compared to 0.2 mM $Ca^{2+}$ needed in the Cea model (see arrows in Fig. 7).

In the CSC filter, the structural oxygen ions form a spontaneous flexible coordinating structure with the counterions (Fig. 8). The filter accumulates a significant amount of $Ca^{2+}$ when the bath contains $10^{-6}$ M $Ca^{2+}$. Also, $Na^{+}$ distribution is substantially modified when 1 $\mu$M $Ca^{2+}$ is added to the baths.

The Cea and CSC models differ in their treatment of both their excluded volume and electrostatics. In the CSC model all the charge of the oxygen ions (-4e) contributes to the electrical flux ($\int \mathbf{E}\cdot\mathbf{n}dA$) in the pore, but in the Cea model only part of the electrical flux produced by the structural charge of the filter (-3.244e) enters the pore because of the peripheral position of these charges (Fig. 1). Neutralization of the larger electrical flux of the CSC model requires a larger ionic countercharge in the pore than in the Cea model. Figure 7, however, shows that the number of cations attracted into the filter regions of both models asymptotes toward similar values in the zero calcium and millimolar calcium regimes. On the other hand, the CSC filter attracts a substantial countercharge to the regions just outside the filter in both the zero calcium and millimolar calcium regimes (Fig. 8). In the CSC model, neither $Ca^{2+}$ nor $Na^{+}$ are able to neutralize the filter charge locally because a strong excluded-volume repulsion counteracts electrostatic attraction. In the Cea model, signs of exclusion from the filter are virtually absent (Fig. 6). Thus we observe, in the CSC model, both stronger electrostatic attraction and stronger excluded-volume repulsion than in the Cea model. The net result (Fig. 7) is an increased selectivity of the CSC model for $Ca^{2+}$ which carries twice the charge of $Na^{+}$ in about the same particle volume. This interpretation of our simulation results of the CSC model is supported by theoretical analysis: the excluded volume of ions and oxygen ions (7, 8, 12) is an

important determinant of selectivity.[3]

## Summary

The studies of Cea have been presented widely in several journals and at different meetings. Because of the bold claims of Cea and the unsubstantiated nature of their extrapolation, an independent investigation is essential. We have performed MC simulations for the Cea model channel. We have constructed an accurate representation of their model and obtained good agreement in computations of energy and of channel occupancy with pure bath solutions for which they report BD results. In addition, we have made GC ensemble simulations for $Ca^{2+}$ concentrations as low as $10^{-6}$ M in the presence of 150 mM $Na^{+}$. These simulations reveal a $Ca^{2+}$ affinity that is much weaker than the Cea extrapolation would suggest and that is much less than the affinity commonly ascribed to the L-type Ca channel. Placement of the structural elements of the channel within the filter (the CSC model of the EEEE locus) improves the calcium selectivity by 40 fold. Reconsideration of other features of the Cea model including a dielectric barrier of excessive magnitude may also be warranted. Regarding the mechanism for high $Ca^{2+}$ selectivity, volume exclusion among the ions and the glutamate oxygens is an integral part of the function of Ca channels that should not be ignored.

## Acknowledgments

The support of the National Institutes of Health (grant No. GM076013 to B.E. and grant No. GM067241 to BE and DG) and the Hungarian National Research Fund (OTKA K63322, to DB) are gratefully acknowledged. A generous allotment of computer time by the Ira and

[3]Yang et al. (42) have made an applied-field molecular dynamics (MD) study of a model calcium channel using a molecular model of water and crude atomistic channel protein. This work is occasionally cited as indicating that with molecular water the CSC mechanism does not lead to calcium selectivity. However, this work was directed to the study of permeation and not selectivity. MD studies inevitably involve shorter chains of events because velocities as well as positions must be updated. Including water molecules only adds to this problem and restricts the study to relatively high ion concentrations. In principle, MD can be performed in the GC ensemble by means of a constraint but this was not done in the study of Yang et al., nor did their MD simulation include methods equivalent to the preference sampling that has been essential in our work. Lastly, we note that the effect of the dielectric coefficient of the protein and membrane was not considered. As a result of these considerations, the valuable Yang et al. study is not relevant to selectivity and was not claimed to be by the authors.

Marylou Fulton Supercomputing Center at BYU is acknowledged with thanks.

## References

1. Hille, B., 2001. Ionic Channels of Excitable Membranes. Sinauer Associates, Sunderland, MA.

2. Almers, W., E. McCleskey, and P. Palade, 1984. Non-selective cation conductance in frog muscle membrane blocked by micromolar external calcium ions. *J. Physiol.* 353:565–583.

3. Almers, W., and E. McCleskey, 1984. Non-selective conductance in calcium channels of frog muscle: Calcium selectivity in a single-file pore. *J. Physiol.* 353:585–608.

4. Ellinor, P., J. Yang, W. Sather, J. Zhang, and R. Tsien, 1995. $Ca^{2+}$ channel selectivity at a single locus for high-affinity $Ca^{2+}$ interactions. *Neuron* 15:1121–1132.

5. Yang, J., P. Ellinor, W. Sather, J. Zhang, and R. Tsien, 1993. Molecular determinants of $Ca^{2+}$ selectivity and ion permeation in L-type $Ca^{2+}$ channels. *Nature* 366:158–161.

6. Sather, W., and E. McCleskey, 2003. Permeation and selectivity in calcium channels. *Annu. Rev. Physiol.* 65:133–159.

7. Nonner, W., L. Catacuzzeno, and B. Eisenberg, 2000. Binding and selectivity in L-type Ca channels: A mean spherical approximation. *Biophys. J.* 79:1976–1992.

8. Nonner, W., D. Gillespie, D. Henderson, and B. Eisenberg, 2001. Ion accumulation in a biological calcium channel: Effects of solvent and confining pressure. *J. Phys. Chem. B* 105:6427–6436.

9. Boda, D., W. Nonner, M. Valiskó, D. Henderson, B. Eisenberg, and D. Gillespie, 2007. Steric selectivity in Na channels arising from protein polarization and mobile side chains. *Biophys. J.* 93:1960–1980.

10. Boda, D., D. Busath, B. Eisenberg, D. Henderson, and W. Nonner, 2002. Monte Carlo simulations of ion selectivity in a biological $Na^{+}$ channel: Charge-space competition. *Phys. Chem. Chem. Phys.* 4:5154–5160.

11. Barker, J., and D. Henderson, 1976. What is "liquid"? Understanding the states of matter. *Rev. Mod. Phys.* 48:587–671.

12. Gillespie, D., 2008. Energetics of divalent selectivity in a calcium channel: The ryanodine receptor case study. *Biophys. J.* In press, doi:10.1529/biophysj.107.116798.

13. Gillespie, D., L. Xu, Y. Wang, and G. Meissner, 2005. (De)constructing the ryanodine receptor: Modeling ion permeation and selectivity of the calcium release channel. *J. Phys. Chem. B* 109:15598–15610.

14. Boda, D., D. Henderson, and D. Busath, 2002. Monte Carlo study of the selectivity of calcium channels: Improved geometrical mode. *Mol. Phys.* 100:2361–2368.

15. Boda, D., D. Henderson, and D. Busath, 2001. Monte Carlo study of the effect of ion and channel size on the selectivity of a model calcium channel. *J. Phys. Chem. B* 105:11574–11577.

16. Boda, D., D. Busath, D. Henderson, and S. Sokołowski, 2000. Monte Carlo simulations of the mechanism of channel selectivity: The competition between volume exclusion and charge neutrality. *J. Phys. Chem. B* 104:8903–8910.

17. Boda, D., M. Valiskó, B. Eisenberg, W. Nonner, D. Henderson, and D. Gillespie, 2007. The combined effect of pore radius and protein dielectric coefficient on the selectivity of a calcium channel. *Phys. Rev. Lett.* 98:168102.

18. Boda, D., M. Valiskó, B. Eisenberg, W. Nonner, D. Henderson, and D. Gillespie, 2006. The effect of protein dielectric coefficient on the ionic selectivity of a calcium channel. *J. Chem. Phys.* 125:034901.

19. Corry, B., T. Allen, S. Kuyucak, and S. Chung, 2001. Mechanisms of permeation and selectivity in calcium channels. *Biophys. J.* 80:195–214.

20. Krishnamurthy, V., and S. Chung, 2007. Large-scale dynamical models and estimation for permeation in biological membrane ion channels. *Proceedings of the IEEE* 95:853–880.

21. Corry, B., and S. Chung, 2006. Mechanisms of valence selectivity in biological ion channels. *Cell. Mol. Life Sci.* 63:301–315.

22. Corry, B., T. Vora, and S. Chung, 2006. Electrostatic basis of valence selectivity in cationic channels. *Biochimica et Biophysica Acta* 1711:72–86.

23. Corry, B., M. Hoyles, T. Allen, M. Walker, S. Kuyucak, and S. Chung, 2002. Reservoir boundaries in Brownian dynamics simulations of ion channels. *Biophys. J.* 82:1975–1984.

24. Im, W., S. Seefeld, and B. Roux, 2000. A grand canonical Monte Carlo-Brownian dynamics algorithm for simulating ion channels. *Biophys. J.* 79:788–801.

25. Guàrdia, E., and J. Padró, 1996. On the influence of ionic charge on the mean force potential of ion pairs in water. *J. Chem. Phys.* 104:7219–7222.

26. Guàrdia, E., R. Rey, and J. Padró, 1991. $Na^+$-$Na^+$ and $Cl^-$-$Cl^-$ ion pairs in water: Mean force potentials by constrained molecular dynamics. *J. Chem. Phys.* 95:2823–2831.

27. Guàrdia, E., R. Rey, and J. Padró, 1991. Potential of mean force by constrained molecular dynamics: A sodium chloride ion-pair in water. *Chem. Phys.* 155:187–195.

28. Lyubartsev, A., and A. Laaksonen, 1995. Calculation of the effective interaction potentials from radial distribution functions: a reverse Monte Carlo approach. *Phys. Rev. E* 52:3730–3737.

29. Chung, S., T. Allen, M. Hoyles, and S. Kuyucak, 1999. Permeation of ions across the potassium channel: Brownian dynamics studies. *Biophys. J.* 77:2517–2533.

30. Fawcett, W., 1999. Thermodynamic parameters for the solvation of monatomic ions in water. *J. Phys. Chem. B* 103:11181–11185.

31. Shannon, R., and C. Previtt, 1969. Effective ionic radii in oxides and fluorides. *Acta Crystallogr. B* 25:925–946.

32. Valleau, J., and L. Cohen, 1980. Primitive model electrolytes. I. Grand canonical Monte Carlo computations. *J. Chem. Phys.* 72:5935–5941.

33. Gibbs, J., 1948. Elementary principles of statistical mechanics, Yale University Press, New Haven, Connecticut, chapter 15.

34. Malasics, A., D. Gillespie, and D. Boda, 2008. Simulating prescribed particle densities in the grand canonical ensemble using iterative algorithms. *J. Chem. Phys.* Submitted.

35. Hoyles, M., S. Kuyucak, and S. Chung, 1998. Solutions of Poisson's equation in channel-like geometries. *Computer Phys. Commun.* 115:45–68.

36. Boda, D., D. Gillespie, W. Nonner, D. Henderson, and B. Eisenberg, 2004. Computing induced charges in inhomogeneous dielectric media: Application in a Monte Carlo simulation of complex ionic systems. *Phys. Rev. E Stat. Nonlin. Soft Matter Phys.* 69:046702.

37. Kostyuk, P., S. Mironov, and Y. Shuba, 1983. Two ion-selective filters in the calcium channel of the somatic membrane of mollusk neurons. *J. Membr. Biol.* 76:83–93.

38. Lansman, J., P. Hess, and R. Tsien, 1986. Blockade of current through single calcium channels by $Cd^{2+}$, $Mg^{2+}$, and $Ca^{2+}$. Voltage and concentration dependence of calcium entry into the pore. *J. Gen. Physiol.* 88:321–347.

39. Fukushima, A., and S. Hagiwara, 1985. Currents carried by monovalent cations through calcium channels in mouse neoplastic B lymphocytes. *J. Physiol.* 358:255–284.

40. Nonner, W., D. Chen, and B. Eisenberg, 1998. Anomalous mole fraction effect, electrostatics, and binding in ionic channels. *Biophys. J.* 74:2327–34.

41. Polo-Parada, L., and S. Korn, 1997. Block of N-type calcium channels in chick sensory neurons by external sodium. *J. Gen. Physiol.* 109:693–702.

42. Yang, Y., D. Henderson, and D. Busath, 2003. Applied-field molecular dynamics study of a model calcium channel selectivity filter. *J. Chem. Phys.* 118:4213–4220.

## Figure captions

**Figure 1** Geometries of the Cea model (A) and the CSC model (B). Red spheres represent negative structural charges in the filter. In the Cea model (A) these four charges are in fixed positions and embedded in the protein body, whereas in the CSC model (B) these charges are eight mobile half-charged oxygen ions confined to the filter lumen but free to move inside. Blue and yellow spheres represent charges forming dipoles at the intracellular entrance. Gray and green spheres represent $Ca^{2+}$ and $Na^{+}$ ions, respectively. The surface grid is that used in solving the integral equations of the electrostatics.

**Figure 2** Convergence of the MC simulation of the CEA model toward equilibrium. The average number of $Na^{+}$ (upper panel) and $Ca^{2+}$ (lower panel) ions is plotted versus the index of the attempt. The baths contained $10^{-5}$ M $CaCl_2$ plus 150 mM NaCl.

**Figure 3** Comparison of axial profiles of potential energy in the Cea model. A single probe ion is moved through the pore and allowed to find its minimal-energy position in the cross-section at each axial location. The upper and lower sets of profiles are obtained with the structural charges of the model set to zero or their normal values, respectively. Curves: Cea; symbols: our results.

**Figure 4** Histograms of axial distribution of ions in the Cea model. The pore is axially divided into 30 bins normal to the axis; the ordinate gives the average number of ions per bin. The solid lines and gray-shaded areas represent the MC results.

**Figure 5** The AMFE experiment of Almers et al. (2) compared to simulation results. Top panel: *circles*, experimental currents normalized with respect to the current at $[Ca^{2+}]= 10^{-7.2}$ ($Ca^{2+}$ was added externally); *squares*, BD simulated currents of Cea (normalized to their maximal value); *dashed and dotted lines*, $Na^{+}$ and $Ca^{2+}$ currents, respectively, estimated by Cea using an extrapolation based on BD simulation results obtained with bath $Ca^{2+}$ concentrations $\geq$18 mM. The Cea $Ca^{2+}$ and $Na^{+}$ results are separately normalized (see text). Bottom panel: Summary of our MC simulation results for the Cea model with varied bath concentration of $Ca^{2+}$ and a fixed concentration of 150 mM NaCl. The symbols give the simulated occupancies of the filter region ($10 \leq z \leq 15$ Å). The curves are first-order isotherms; their limiting value at low $Ca^{2+}$ concentration is constrained by a simulation done with $Ca^{2+}$-free baths (point not shown). The arrow marks the concentration where $Na^{+}$ occupancy is reduced to one half that found in the absence of $Ca^{2+}$.

**Figure 6** Axial distributions of ions: MC results. Spatial bins are 0.2 Å wide and normal to the axis. The baths contained 150 mM NaCl plus the indicated concentration of $CaCl_2$. The inset shows $Ca^{2+}$ distributions in the filter at an enlarged scale. Gray shaded areas are shown to help relate the ion distributions to pore geometry.

**Figure 7** Ion accumulation in the CSC and Cea models. Results of MC simulations; ions are counted in the axial range $10 \leq z \leq 15$ Å. *Filled symbols*, CSC model; *Open symbols*, Cea model. The baths contained a fixed concentration of 150 mM NaCl and the indicated concentration of $Ca^{2+}$. The lines represent first-order isotherms; their limiting value at low $Ca^{2+}$ concentration is constrained by simulations done with $Ca^{2+}$-free baths; these $Na^+$ occupancies were 1.562 (Cea) and 1.572 (CSC). Arrows mark concentrations where $Na^+$ occupancy is reduced to one half that found in the absence of $Ca^{2+}$.

**Figure 8** Axial ion distributions in the CSC model. MC results; spatial bins are 0.2 Å wide and normal to the axis. The inset shows the distribution of the oxygen ions inside the filter region. The baths contained 150 mM NaCl plus the indicated concentration of $CaCl_2$. Gray shaded areas are shown to help relate the ion distributions to pore geometry.

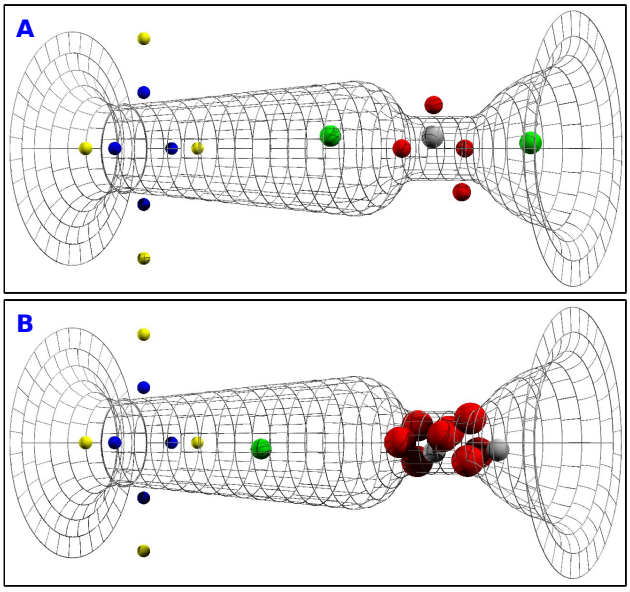


Figure 1:

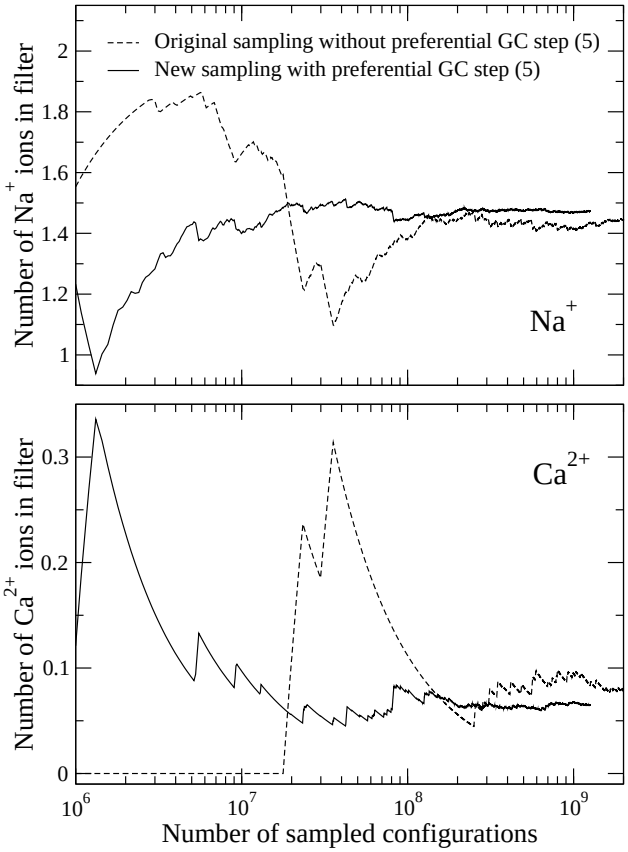
Original sampling without preferential GC step (5)
New sampling with preferential GC step (5)
Number of Na+ ions in filter
Na+
Number of Ca2+ ions in filter
Ca2+
Number of sampled configurations

Figure 2:

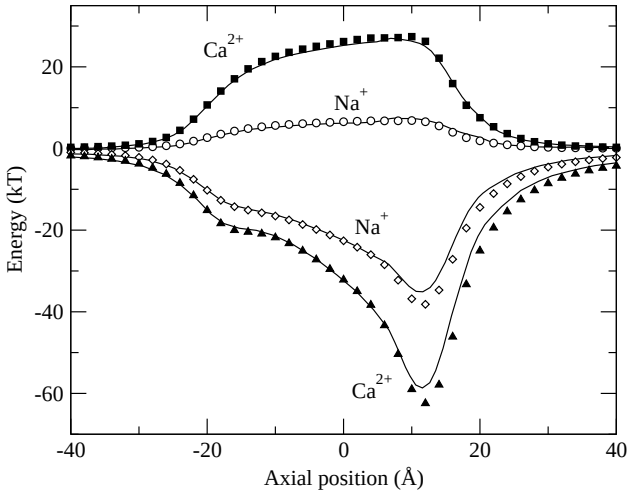
Ca2+
Na+
Na+
Ca2+
20
0
-20
-40
-60
Energy (kT)
-40
-20
0
20
40
Axial position (Å)

Figure 3:

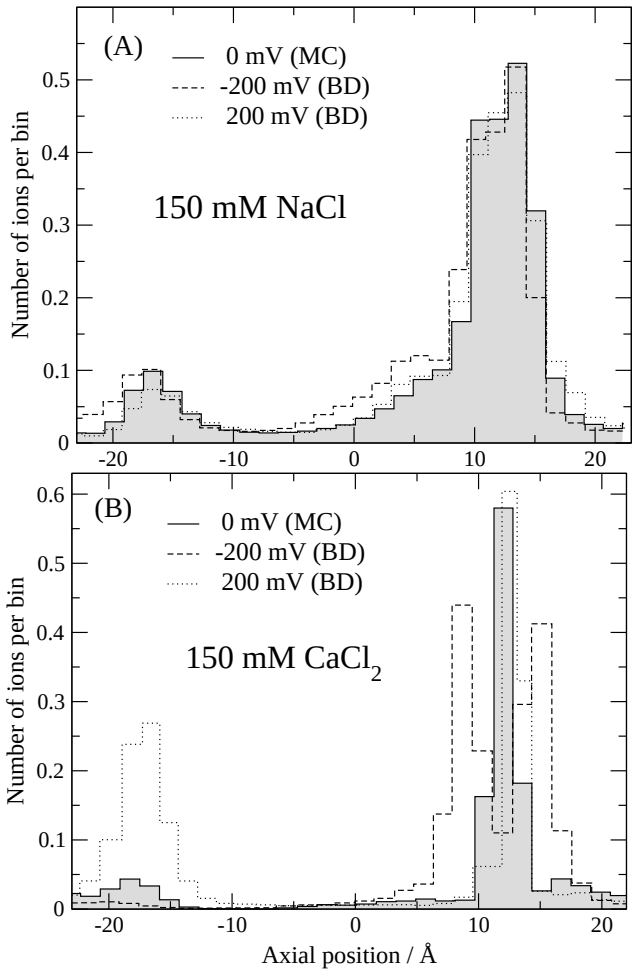
(A)
0 mV (MC)
-200 mV (BD)
200 mV (BD)
150 mM NaCl
Number of ions per bin
0
0.1
0.2
0.3
0.4
0.5
-20
-10
0
10
20
(B)
0 mV (MC)
-200 mV (BD)
200 mV (BD)
150 mM CaCl2
Number of ions per bin
0
0.1
0.2
0.3
0.4
0.5
0.6
-20
-10
0
10
20
Axial position / Å

Figure 4:

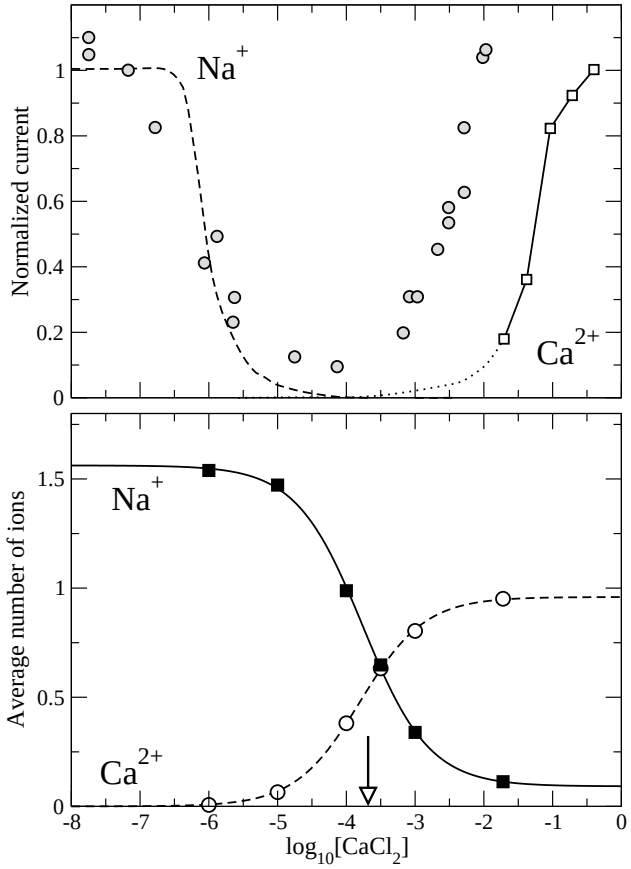
Na+
Ca2+
Normalized current
0
0.2
0.4
0.6
0.8
1
Na+
Ca2+
Average number of ions
0
0.5
1
1.5
-8
-7
-6
-5
-4
-3
-2
-1
0
log10[CaCl2]

Figure 5:

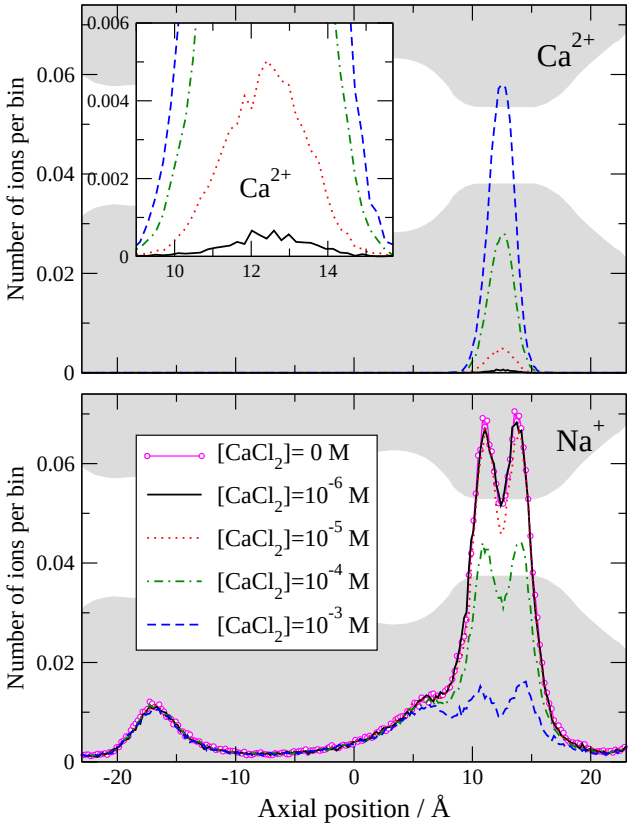
Ca2+
Na+
Number of ions per bin
Axial position / Å
[CaCl2]= 0 M
[CaCl2]=10-6 M
[CaCl2]=10-5 M
[CaCl2]=10-4 M
[CaCl2]=10-3 M

Figure 6:

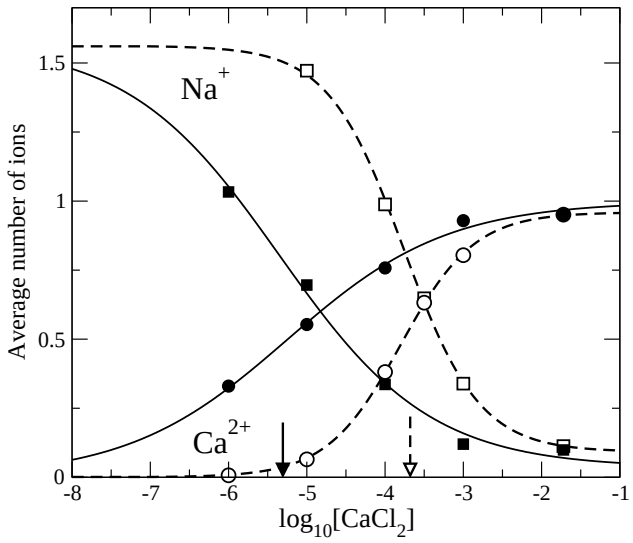


Figure 7:

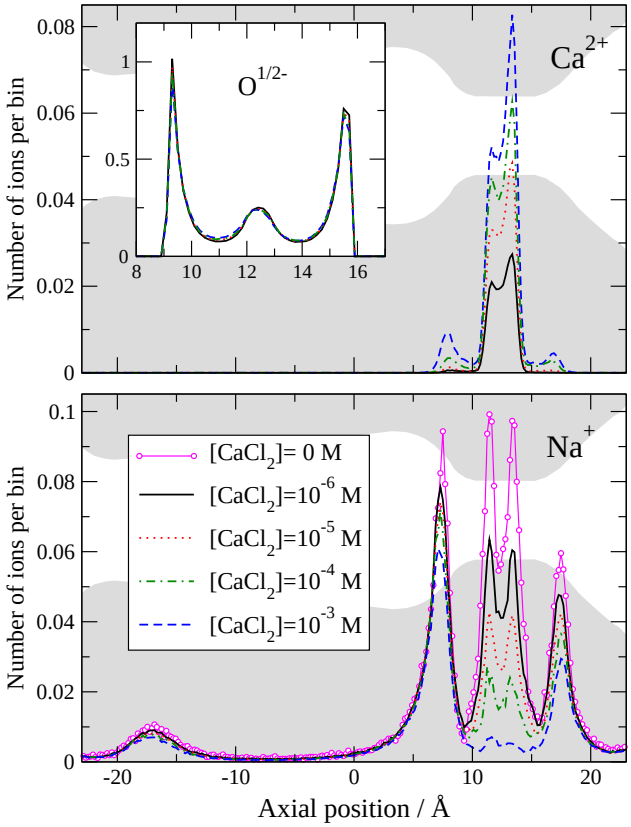
Ca2+
O1/2-
Na+
[CaCl2]= 0 M
[CaCl2]=10-6 M
[CaCl2]=10-5 M
[CaCl2]=10-4 M
[CaCl2]=10-3 M
Number of ions per bin
Axial position / Å

Figure 8: